Proof: Let the group delay [5] of $\Lambda(\omega)$ be

$$\tau(\omega) = \theta'(\omega) = \sum_{n=-\infty}^{+\infty} d_n e^{jn\omega}.$$

Taking derivative of (14) with respect to ω, we get

$$\tau(\omega - \pi) - \frac{1}{2}\tau\left(\frac{\omega}{2}\right) - \frac{1}{2}\tau\left(\frac{\omega}{2} - \pi\right) = 0.$$

Substituting the Fourier series representation of $\tau(\omega)$ into the equation above gives

$$\sum_{n=-\infty}^{+\infty} (-1)^n d_n e^{jn\omega} - \frac{1}{2}\sum_{n=-\infty}^{+\infty} [1 + (-1)^n] d_n e^{j(n/2)\omega} = 0$$

or

$$\sum_{n=-\infty}^{+\infty} [(-1)^n d_n - d_{2n}] e^{jn\omega} = 0.$$

Therefore

$$d_{2n} = (-1)^n d_n, \ n \neq 0.$$

Since $\{d_n\}$ is the Fourier series coefficients of $\tau(\omega)$, the limit of the subsequence

$$\{d_n, d_{2n}, d_{2^2n}, d_{2^3n}, \ldots\} = \{d_n, (-1)^n d_n, (-1)^n d_n, (-1)^n d_n, \ldots\}$$

is equal to zero for any $n \neq 0$. Thus, $\tau(\omega) = d_0$, and therefore $\theta(\omega) = d_0\omega + \theta_0$, for $|\omega| < \pi$. It then follows from the phase condition (14) with (15) that $\theta(\omega) = \omega/2$. The proof is complete. ■

Combining Propositions 1 and 2, we see that the unique solution to the Hilbert transform pair condition (8) (or (9) with (10)) is given as follows:

$$\Lambda(\omega) = e^{-j(\omega/2)}, \ |\omega| < \pi.$$

We now can summarize the main result on Hilbert transform pairs of orthogonal wavelet bases as follows.

Theorem 2: Two orthogonal wavelet bases form Hilbert transform pairs if and only if the scaling filters are offset from one another by a half sample; that is, the two filters must have the same magnitude response and their phases must be shifted by half a sample. Specifically, they are related by

$$G_0(\omega) = e^{-j(\omega/2)} H_0(\omega), \ |\omega| < \pi.$$

IV. Conclusion

The forming of Hilbert transform pairs of two scalar orthogonal wavelet bases is re-examined in this note. Necessary and sufficient conditions on scaling filters that render Hilbert transform pairs are derived. The solutions to these conditions are obtained. In addition to the phase condition, the identical magnitude response requirement for the two associated scaling filters is established. The uniqueness of the solution to the Hilbert transform pair condition justify the use of the half-sample delay requirement as a criterion in the design of Hilbert transform pairs of orthogonal wavelets bases.

Acknowledgment

The authors would like to thank the anonymous reviewers for their comments, which helped improve the quality of this correspondence.

References

[1] P. Abry, *Ondelettes et Turbulences*. Paris, France: Diderot, 1997.
[2] P. Abry and P. Flandrin, "Multiresolution transient detection," in *Proc. IEEE-SP Int. Symp. Time-Frequency Time-Scale Analysis*, Philadelphia, PA, Oct. 1994, pp. 225–228.
[3] F. C. Fernandes, I. W. Selesnick, R. L. C. van Spaendonck, and C. S. Burrus, "Complex wavelet transforms with allpass filters," *Signal Process.*, vol. 83, pp. 1689–1706, Aug. 2003.
[4] N. G. Kingsbury, "Image processing with complex wavelets," *Philos. Trans. R. Soc. London A, Math. Phys. Sci.*, vol. 357, pp. 2543–2560, Sep. 1999.
[5] A. V. Oppenheim and R. W. Schafer, *Discrete Time Signal Processing*. Englewood Cliffs, NJ: Prentice-Hall, 1989.
[6] H. Ozkaramanli and R. Yu, "On the phase condition and its solution for Hilbert transform pairs of wavelet bases," *IEEE Trans. Signal Process.*, vol. 51, no. 12, pp. 3293–3294, Dec. 2003.
[7] E. Ozturk, O. Kucur, and G. Atkin, "Waveform encoding of binary signals using a wavelet and its Hilbert transform," in *IEEE Int. Conf. Acoustics, Speech, Signal Processing (ICASSP 2000)*, vol. 5, Istanbul, Turkey, Jun. 2000, pp. 2641–2644.
[8] I. W. Selesnick, "Hilbert transform pairs of wavelets bases," *IEEE Signal Process. Lett.*, vol. 8, no. 6, pp. 170–173, Jun. 2001.
[9] ——, "The design of approximate Hilbert transform pairs of wavelets bases," *IEEE Trans. Signal Process.*, vol. 50, no. 5, pp. 1144–1152, May 2002.
[10] G. Strang and T. Nguyen, *Wavelets and Filter Banks*. Wellesley, MA: Wellesley-Cambridge Press, 1996.
[11] D. B. H. Tay and M. Palaniswami, "Design of approximate Hilbert transform pair of wavelets with exact symmetry," in *IEEE Int. Conf. Acoustics, Speech, Signal Processing (ICASSP 2004)*, vol. 2, Montreal, QC, Canada, May 2004, pp. 921–924.

Local Directional Denoising

S. C. Olhede and A. T. Walden

***Abstract*—Denoising of complex-valued signals involves the relationships between the real and imaginary parts of the signal. The authors introduce the idea of local directional thresholding, well-suited to signals that are bidirectional overall but unidirectional at any one time, such as Doppler ultrasound, and show its efficacy on synthetic and real data.**

***Index Terms*—Complex-valued signal, denoising, Hilbert transform, ultrasound, wavelet transform.**

I. Introduction

Wavelet thresholding [1], [2] has become a standard approach to the denoising of real-valued signals. The discrete wavelet transform is used to transform the noisy signal, on the assumption that the wavelet coefficients of the signal component are sparse and exceed those expected from the noise. The wavelet coefficients are thresholded according to their magnitudes, and the inverse transform is applied to obtain the denoised version of the signal. Circular shift equivariance can be achieved by using the technique of "cycle-spinning" [3]–[5], where the signal extraction procedure is applied not only to the original series but also to

Manuscript received October 6, 2004; revised February 16, 2005. The associate editor coordinating the review of this manuscript and approving it for publication was Dr. Ta-Hsin Li.

The authors are with the Department of Mathematics, Imperial College London, London SW7 2BZ, U.K. (e-mail: s.olhede@imperial.ac.uk and a.walden@imperial.ac.uk).

Digital Object Identifier 10.1109/TSP.2005.859262

all possible circularly shifted series of interest; this is equivalent ([6, p. 429]) to applying standard thresholding to the wavelet coefficients of the maximal-overlap/stationary/shift-invariant discrete wavelet transform.

The success of any thresholding depends on an understanding of the nature of the deterministic signal, and the statistical properties of the noise. We begin with a detailed consideration of the signal. In this correspondence, we look at the denoising of a particularly useful class of *complex-valued* signals. The basic model is that of a complex-valued deterministic signal contaminated with complex Gaussian white noise. Let $\mathbf{d}$ denote the complex-valued column vector consisting of the values of the deterministic signal, and $\boldsymbol{\epsilon}$ denote the complex-valued noise vector, so that the observed data vector $\mathbf{z}$ is given by $\mathbf{z} = \mathbf{d} + \boldsymbol{\epsilon}$.

The real and imaginary parts of complex-valued signals can arise in several ways, such as the following:

1) from two different signals where there is no special relationship between the components;
2) as two channels from a multichannel recording, representing the two components of polarized motion—e.g., the radial and vertical recordings of Rayleigh waves in an earthquake coda [7] (in this case, the real and imaginary parts would be physically closely related);
3) directly as components of a complex-valued recording. (In quadrature Doppler ultrasound [8, p. 89], the signal is backscattered from the ultrasound beam by moving red blood cells, and the Doppler effect is used to measure the velocity of blood flow; femoral artery blood flow is in reverse directions during heart contraction and dilation).

Our interest will be directed toward complex-valued signals carrying directional information localized in time. As an example of a locally directional signal, we consider a complex-valued blood flow record $\mathbf{z}$ from *in-vivo* longitudinal Doppler ultrasound measurements on the hepatic vein of a 33-year-old male. The sampling interval used was 0.5 ms. It is shown in Fig. 1(a). At the beginning and end of the signal, the imaginary part lags the real part, while in the middle, the imaginary part leads the real part. This is characteristic of the presence of two different flow directions, forward at the beginning and end, and reverse in the middle.

Let us first think about the global directionality of a signal. Let $\{D_k, k = 0, \ldots, N-1\}$ be the discrete Fourier transform (DFT) of the complex-valued signal $\{d_t, t = 0, \ldots, N-1\}$. The DFT of the reversed signal $\{\tilde{D}_k, k = 0, \ldots, N-1\}$ is given by $\tilde{D}_k = \sum_{t=0}^{N-1} d_{-t} e^{-i2\pi tk/N}$, so that

$$\tilde{D}_k = \sum_{t=0}^{N-1} \left[\left(\frac{1}{N} \right) \sum_{l=0}^{N-1} D_l e^{i2\pi(-t)l/N} \right] e^{-i2\pi tk/N}$$
$$= \left(\frac{1}{N} \right) \sum_{l=0}^{N-1} D_l \left[\sum_{t=0}^{N-1} e^{-i2\pi t(l+k)/N} \right] = D_{N-k}.$$

If $f_k = k/N$, $k = (N/2)+1, \ldots, N-1$, correspond to negative Fourier frequencies, then $(N-k)/N$ corresponds to positive frequencies, and so reversing the time direction corresponds to mapping frequency behavior at f_k to $-f_k$. Hence, directionality can be related to analytic signals, supported on positive frequencies only, and antianalytic signals, supported on negative frequencies only [9].

Fig. 2 shows the time–frequency spectrogram of the signal, i.e., the local frequency content of the signal at any time, computed using a zeroth-order Hermite window [10, p. 298]. The positive frequency energy is associated with forward flow, and the negative with reverse flow. We conclude that basically the signal is bidirectional overall but unidirectional at any one time.

Our approach to denoising of locally directional noisy signals is to first split the data into analytic and antianalytic components. Where the signal is locally forward directional, it will appear in the analytic vector $\mathbf{z}^+$, and where it is locally reverse directional, it will appear in the antianalytic vector $\mathbf{z}^-$ [see Fig. 1(b) and (c)]. (The calculation of $\mathbf{z}^+$ and $\mathbf{z}^-$ is discussed in Section II.) We then apply the maximal-overlap discrete wavelet transform (MODWT) and hard threshold the forward, $W_{j,t}^{(\mathbf{z}^+)}$, and reverse, $W_{j,t}^{(\mathbf{z}^-)}$, noisy wavelet coefficients, according to their magnitudes, and reconstruct the deterministic signal as the average of the two directional reconstructions. White noise spreads evenly across positive and negative frequencies, and for those times when the signal is forward directional, energy in $W_{j,t}^{(\mathbf{z}^-)}$ will be noise

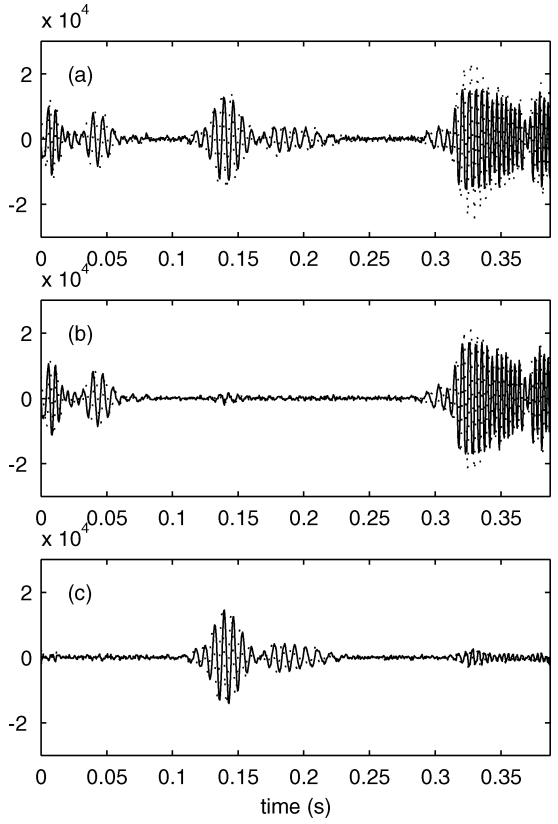

Fig. 1. Decomposition of complex-valued hepatic vein data into analytic and antianalytic components. In each plot, the solid line is the real part, and the dotted line is the imaginary part: (a) the recorded signal, (b) analytic component $\mathbf{z}^+/2$, and (c) antianalytic component $\mathbf{z}^-/2$. The sum of (b) and (c) gives (a).

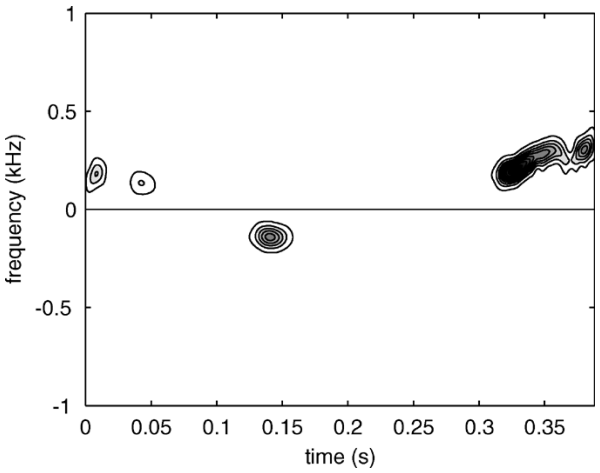

Fig. 2. Hermite window spectrogram of the hepatic vein data.

and can be removed, and for those times when the signal is reverse directional, energy in $W_{j,t}^{(\mathbf{z}^+)}$ will be noise and can be deleted, so that our approach should effectively eliminate half the noise. This is due to properties of universal thresholding applied to pure noise wavelet coefficients, with one of the two directional components consisting only of noise. (If the signal is not locally directional, then no advantage will accrue from the additional steps; however, the wavelet transform will still unbalance the energy in both directions and act in a manner similar to standard denoising.)

We now give details of the steps involved, and statistical results on the behavior of the noise.

II. Analytic and Anti-Analytic Components

Given a complex-valued vector $\mathbf{z} = [z_0, \ldots, z_{N-1}]^T$, with N assumed even throughout, we denote the discrete Hilbert transform (DHT) of $\mathbf{z}$ by $\mathcal{H}\mathbf{z}$, where $\mathcal{H}$ is the DHT matrix [11], [12]. Let $\mathbf{z} = \mathbf{x} + i\mathbf{y}$. We define

$$\mathbf{z}^{\pm} = \mathbf{z} \pm i\mathcal{H}\mathbf{z} = \mathbf{x} \mp \mathcal{H}\mathbf{y} + i(\mathbf{y} \pm \mathcal{H}\mathbf{x}). \tag{1}$$

The action of $\mathcal{H}$ is best understood in the frequency domain. The DFT of $\mathbf{z}^+/\mathbf{z}^-$ consists of taking the Fourier coefficients of $\mathbf{z}$ and doubling them for positive/negative Fourier frequencies, leaving them untouched for zero and Nyquist frequency, and zeroing them for negative/positive frequencies, i.e., if $\{Z_k, k = 0, \ldots, N-1\}$ is the DFT of $\{z_t, t = 0, \ldots, N-1\}$, then

$$Z_k^+ = \begin{cases} Z_k, & k = 0,\ \frac{N}{2} \\ 2Z_k, & k = 1, \ldots,\ \frac{N}{2} - 1, \\ 0, & k = \frac{N}{2} + 1, \ldots, N-1, \end{cases}$$

and

$$Z_k^- = \begin{cases} Z_k, & k = 0,\ \frac{N}{2} \\ 0, & k = 1, \ldots,\ \frac{N}{2} - 1, \\ 2Z_k, & k = \frac{N}{2} + 1, \ldots, N-1. \end{cases}$$

We recall that the decomposition $\mathbf{z} = \mathbf{x} + i\mathbf{y} = (1/2)\left(\mathbf{z}^+ + \mathbf{z}^-\right)$, is illustrated in Fig. 1(b) and (c).

III. Wavelet Transformation and Thresholding

A. Nondecimated Discrete Wavelet Transformation

Suppose we apply the MODWT to $\mathbf{z}$. This is overdetermined and also known variously as a stationary or shift-invariant or nondecimated transform. At level $j = J_0$ of the transform, we have N-length wavelet coefficient vectors $\mathbf{W}_1^{(\mathbf{z})}, \ldots, \mathbf{W}_{J_0}^{(\mathbf{z})}$ and a single scaling coefficient vector $\mathbf{V}_{J_0}^{(\mathbf{z})}$, given by $\mathbf{W}_j^{(\mathbf{z})} = \mathcal{W}_j\mathbf{z}$, $j = 1, \ldots, J_0$, and $\mathbf{V}_{J_0}^{(\mathbf{z})} = \mathcal{V}_{J_0}\mathbf{z}$, where $\mathcal{W}_j$ and $\mathcal{V}_{J_0}$ are $N \times N$ filter matrices of the form described in [6, p. 171]; the filters involved are all real-valued. If the basic scaling and wavelet filters have L coefficients, then the rows of $\mathcal{W}_j$ and $\mathcal{V}_{J_0}$ are constructed from filters with $L_j = (2^j - 1)(L-1) + 1$ coefficients. Let $\{W_{j,t}^{(\mathbf{z})}, t = 0, \ldots, N-1\}$ denote the elements of $\mathbf{W}_j^{(\mathbf{z})}$. Clearly, also $\mathbf{W}_j^{(\mathbf{z})} = \mathcal{W}_j\mathbf{z} = \mathcal{W}_j\mathbf{d} + \mathcal{W}_j\boldsymbol{\epsilon} = \mathbf{W}_j^{(\mathbf{d})} + \mathbf{W}_j^{(\boldsymbol{\epsilon})}$. The vector $\mathbf{z}$ can be reconstructed via

$$\mathbf{z} = \sum_{j=1}^{J_0} \mathcal{W}_j^T\mathbf{W}_j^{(\mathbf{z})} + \mathcal{V}_{J_0}^T\mathbf{V}_{J_0}^{(\mathbf{z})}. \tag{2}$$

Now, $\mathbf{z} = \mathbf{x} + i\mathbf{y} = (1/2)\left(\mathbf{z}^+ + \mathbf{z}^-\right)$, and so from (2)

$$\mathbf{z} = \frac{1}{2}\sum_{j=1}^{J_0} \mathcal{W}_j^T\left(\mathbf{W}_j^{(\mathbf{z}^+)} + \mathbf{W}_j^{(\mathbf{z}^-)}\right) + \mathcal{V}_{J_0}^T\mathbf{V}_{J_0}^{(\mathbf{z})}. \tag{3}$$

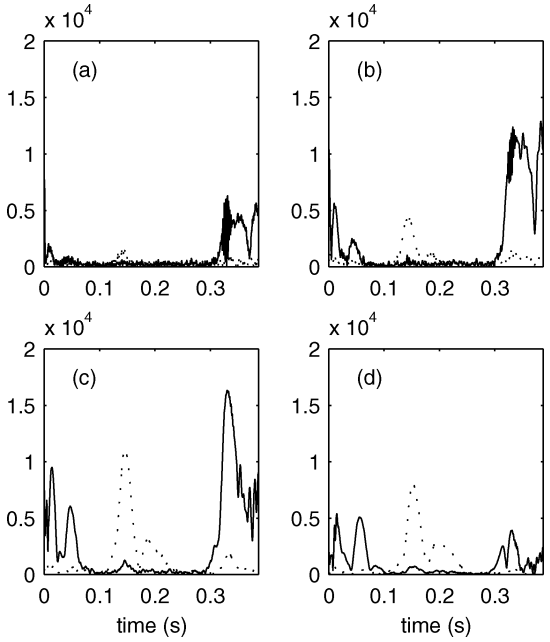

Fig. 3. Analysis of hepatic vein data. (a)–(d) Absolute values of MODWT coefficient vectors, $\left|(1/2)\mathbf{W}_j^{(\mathbf{z}^+)}\right|$ for $j = 1, \ldots, 4$, respectively (solid lines), and $\left|(1/2)\mathbf{W}_j^{(\mathbf{z}^-)}\right|$ for $j = 1, \ldots, 4$, respectively (dotted lines).

For the hepatic vein data, Fig. 3(a)–(d) shows $\left|(1/2)\mathbf{W}_j^{(\mathbf{z}^+)}\right|$ for $j = 1, \ldots, 4$, respectively, as solid lines, and $\left|(1/2)\mathbf{W}_j^{(\mathbf{z}^-)}\right|$ for $j = 1, \ldots, 4$, respectively, as dotted lines. We note that whenever large coefficients occur, the forward component either dominates the reverse component, or vice versa.

B. Sparseness and Thresholding

The idea of sparsity when thresholding *real-valued* noisy signals is that a relatively few wavelet coefficients carry most of the energy in the signal [2], and the universal thresholding strategy was developed with this property in mind. Two different notions of sparsity of a vector of wavelet coefficients were suggested in [13]:

1) Only a small proportion of wavelet coefficients are nonzero.
2) The ordered amplitudes of the wavelet coefficients obey a power law.

The amplitude of a complex quantity is well defined, and so these measures of sparsity can be applied to complex coefficients, as is implicit in [14]. Spatial adaptivity will apply to the complex case, with the complex signal considered as a single entity, rather than two separate ones (the real and imaginary parts), and will refer to the local (in time) smoothing of the complex vector.

We shall consider the first of the two notions of sparsity in terms of the particular form arising from the local directionality introduced earlier. We assume that the deterministic components of $\mathbf{z}^+$ and $\mathbf{z}^-$, namely $\mathbf{d}^+$ and $\mathbf{d}^-$, respectively, are complex-valued signals existing in a suitable smoothness space [2]. This simply corresponds to assuming that the signal $\mathbf{d}$ is a sum of suitably smooth signals with local directionality, where $\mathbf{d}^+$ and $\mathbf{d}^-$ separately satisfy the same criteria as those signals considered by Sardy in [14]. Hence, for locally directional signals and appropriate values of the doublet (j,t), it follows that $W_{j,t}^{(\mathbf{d}^+)} \neq 0$, $W_{j,t}^{(\mathbf{d}^-)} = 0$, and vice versa; in this instance, $W_{j,t}^{(\mathbf{d})} \neq 0$, and neither the real nor imaginary part of this quantity need be zero.

We thus threshold the forward $W_{j,t}^{(\mathbf{z}^+)}$ and reverse $W_{j,t}^{(\mathbf{z}^-)}$ directional versions of the noisy wavelet coefficients separately according

to their magnitudes, obtaining $\widehat{W}_{j,t}^{(\mathbf{z}^+)}$ and $\widehat{W}_{j,t}^{(\mathbf{z}^-)}$, respectively, and reconstruct the deterministic signal as the average of the two reconstructions:

$$\hat{\mathbf{z}} = \frac{1}{2}\sum_{j=1}^{J_0} \mathcal{W}_j^T \left[\widehat{\mathbf{W}}_j^{(\mathbf{z}^+)} + \widehat{\mathbf{W}}_j^{(\mathbf{z}^-)}\right] + \mathcal{V}_{J_0}^T \mathbf{V}_{J_0}^{(\mathbf{z})}. \tag{4}$$

We shall call this *local directional thresholding*. Notice that this approach, applied to complex-valued signals, using real-valued wavelet filters, gives rise to multiple (two) wavelet coefficients—the real and imaginary parts—at each (j,t). Multiple wavelet coefficients are created in [15] by using multiwavelets, and in [16], by using complex-valued wavelet filters, but in both cases applied to a real-valued signal; these approaches are fundamentally different to ours, since we seek to exploit the physical relationship between the real and imaginary parts of the complex-valued signal.

IV. Noise Statistics

Thresholding is designed under the assumption of the absence of signal, $\mathbf{z} = \boldsymbol{\epsilon}$, and it is the properties of the noise that determine the appropriate threshold.

A. The Noise Model

We shall use an isotropic noise structure for the complex vector $\boldsymbol{\epsilon} = \boldsymbol{\epsilon}_1 + i\boldsymbol{\epsilon}_2$, namely, $[\boldsymbol{\epsilon}_1, \boldsymbol{\epsilon}_2]^T \sim \mathcal{N}_{2N}(\mathbf{0}, (\sigma_\epsilon^2/2)\mathbf{I})$, i.e., the vector has the same distribution as a real $2N$-vector-valued Gaussian random variable with mean $\mathbf{0}$ and covariance matrix $(\sigma_\epsilon^2/2)\mathbf{I}$. Hence, both the real and imaginary noise components consist of uncorrelated Gaussian white noise with semivariance $\sigma_\epsilon^2/2$, with zero correlation between them.

B. Local Directional Thresholding

Let $\boldsymbol{\eta}^\pm = \boldsymbol{\epsilon} \pm i\mathcal{H}\boldsymbol{\epsilon} = (\mathbf{I} \pm i\mathcal{H})\boldsymbol{\epsilon}$. Note that since $\boldsymbol{\epsilon}$ is complex, $(\boldsymbol{\eta}^+)^* \neq \boldsymbol{\eta}^-$, where * denotes complex-conjugate. Then, with ^{H} denoting Hermitian transpose

$$\begin{aligned} E\{\boldsymbol{\eta}^\pm[\boldsymbol{\eta}^\pm]^H\} &= E\{(\mathbf{I} \pm i\mathcal{H})\boldsymbol{\epsilon}\boldsymbol{\epsilon}^H(\mathbf{I} \mp i\mathcal{H}^T)\} \\ &= \sigma_\epsilon^2\left[(\mathbf{I} + \mathcal{H}\mathcal{H}^T) \pm i(\mathcal{H} - \mathcal{H}^T)\right]. \end{aligned}$$

$\mathcal{H}\mathcal{H}^T$ is a symmetric Toeplitz matrix with first row $[1-(2/N), 0, -(2/N), 0, -(2/N), \ldots, -(2/N), 0]$, so $\mathcal{H}\mathcal{H}^T = \mathbf{I}$ to $O(1/N)$ and since $\mathcal{H}$ is skew-symmetric, we have that $\mathcal{H}^T = -\mathcal{H}$, so that, asymptotically

$$E\{\boldsymbol{\eta}^\pm[\boldsymbol{\eta}^\pm]^H\} = 2\sigma_\epsilon^2[\mathbf{I} \pm i\mathcal{H}]. \tag{5}$$

The principal diagonal of $\mathcal{H}$ is identically all zeros [11] so that the variances along the principal diagonal of $E\{\boldsymbol{\eta}^\pm[\boldsymbol{\eta}^\pm]^H\}$ are well defined. Since $\boldsymbol{\epsilon}$ is complex Gaussian, $E\{\boldsymbol{\epsilon}\boldsymbol{\epsilon}^T\} = \mathbf{0}$, and so $E\{\boldsymbol{\eta}^\pm[\boldsymbol{\eta}^\pm]^T\} = E\{(\mathbf{I} \pm i\mathcal{H})\boldsymbol{\epsilon}\boldsymbol{\epsilon}^T(\mathbf{I} \pm i\mathcal{H}^T)\} = \mathbf{0}$. Hence, asymptotically, $\boldsymbol{\eta}^\pm$ has a complex Gaussian distribution with covariance matrix (5), i.e., $\boldsymbol{\eta}^\pm \sim \mathcal{N}_N^C(\mathbf{0}, 2\sigma_\epsilon^2[\mathbf{I} \pm i\mathcal{H}])$. The cross-covariance $E\{\boldsymbol{\eta}^+[\boldsymbol{\eta}^-]^H\}$ is $\sigma_\epsilon^2[(\mathbf{I} - \mathcal{H}\mathcal{H}^T)]$ so that the cross-covariance matrix will be null asymptotically. Contrarily, the complementary cross-covariance $E\{\boldsymbol{\eta}^+[\boldsymbol{\eta}^-]^T\}$ is identically zero for all N. Note that $\boldsymbol{\eta}^+$ and $\boldsymbol{\eta}^-$ are each formed from correlated complex-valued random variables, but that, asymptotically, these two vectors of random variables are uncorrelated with each other.

The real $\boldsymbol{\eta}_1^\pm = \Re\{\boldsymbol{\eta}^\pm\}$ and imaginary $\boldsymbol{\eta}_2^\pm = \Im\{\boldsymbol{\eta}^\pm\}$ parts of $\boldsymbol{\eta}^\pm$ have covariances given by

$$E\{\boldsymbol{\eta}_1^\pm(\boldsymbol{\eta}_2^\pm)^T\} = E\{(\boldsymbol{\epsilon}_1 \mp \mathcal{H}\boldsymbol{\epsilon}_2)(\boldsymbol{\epsilon}_2^T \pm \boldsymbol{\epsilon}_1^T\mathcal{H}^T)\} = \mp\sigma_\epsilon^2\mathcal{H}$$

and $E\{\boldsymbol{\eta}_2^\pm(\boldsymbol{\eta}_1^\pm)^T\} = -E\{\boldsymbol{\eta}_1^\pm(\boldsymbol{\eta}_2^\pm)^T\}$. Again, since the principal diagonal of $\mathcal{H}$ is all zeros, we see that the real and imaginary parts are uncorrelated at any time t, i.e., $E\{\eta_{1,t}^\pm \eta_{2,t}^\pm\} = 0$. Further

$$E\{\boldsymbol{\eta}_1^\pm(\boldsymbol{\eta}_1^\pm)^T\} = E\{\boldsymbol{\eta}_2^\pm(\boldsymbol{\eta}_2^\pm)^T\} = \left(\frac{\sigma_\epsilon^2}{2}\right)(\mathbf{I} + \mathcal{H}\mathcal{H}^T)$$

which is asymptotically equal to $\sigma_\epsilon^2\mathbf{I}$, and

$$E\{\boldsymbol{\eta}_1^+(\boldsymbol{\eta}_1^-)^T\} = E\{\boldsymbol{\eta}_2^+(\boldsymbol{\eta}_2^-)^T\} = \left(\frac{\sigma_\epsilon^2}{2}\right)(\mathbf{I} - \mathcal{H}\mathcal{H}^T)$$

which is asymptotically equal to $\mathbf{0}$.

Applying the MODWT to $\mathbf{z}^\pm$ in the absence of signal, we obtain, at level j

$$\mathbf{W}_j^{(\mathbf{z}^\pm)} = \mathcal{W}_j(\boldsymbol{\eta}_1^\pm + i\boldsymbol{\eta}_2^\pm) = \mathbf{n}_{j1}^\pm + i\mathbf{n}_{j2}^\pm$$

say. Now

$$\begin{aligned} \operatorname{cov}\{\mathbf{n}_{j1}^\pm, \mathbf{n}_{j2}^\pm\} &= E\{\mathbf{n}_{j1}^\pm(\mathbf{n}_{j2}^\pm)^T\} = \mathcal{W}_j E\{\boldsymbol{\eta}_1^\pm(\boldsymbol{\eta}_2^\pm)^T\}\mathcal{W}_j^T \\ &= \pm\sigma_\epsilon^2\mathcal{W}_j\mathcal{H}^T\mathcal{W}_j^T. \end{aligned} \tag{6}$$

Further, $E\{\mathbf{n}_{j1}^\pm(\mathbf{n}_{j1}^\pm)^T\} = \mathcal{W}_j E\{\boldsymbol{\eta}_1^\pm(\boldsymbol{\eta}_1^\pm)^T\}\mathcal{W}_j^T$, which is asymptotically equal to $\sigma_\epsilon^2\mathcal{W}_j\mathcal{W}_j^T$, and likewise for $E\{\mathbf{n}_{j2}^\pm(\mathbf{n}_{j2}^\pm)^T\}$. Again, since the diagonal elements of the matrix in (6) are zero, the Gaussian random variables $n_{j1,t}^\pm$ and $n_{j2,t}^\pm$ are independent at any time t, with mean zero and variance $\sigma_{n_j}^2 = \sigma_\epsilon^2/2^j$ to $O(1/N)$, and j such that $L_j \leq N$ (see [17]).

Hence, asymptotically, $\left\{\left|W_{j,t}^{(\mathbf{z}^\pm)}/\sigma_{n_j}\right|^2\right\}$ is a series of correlated χ_2^2 random variables. Now, $\sqrt{[2\log(N\log N)]}$ provides a conservative threshold for these correlated chi-square variables [14], [17], so we arrive at the thresholding scheme

$$\widehat{W}_{j,t}^{(\mathbf{z}^\pm)} = \begin{cases} W_{j,t}^{(\mathbf{z}^\pm)}, & \text{if } \frac{|W_{j,t}^{(\mathbf{z}^\pm)}|}{\sigma_{n_j}} > \sqrt{[2\log(N\log N)]} \\ 0, & \text{otherwise.} \end{cases} \tag{7}$$

V. Examples

In this section, we shall compare our local directional thresholding with three alternative methods.

A. Alternative Approaches

The first is what we shall call *standard thresholding* and consists of separately thresholding the real $W_{j,t}^{(\Re\{\mathbf{z}\})}$ and imaginary $W_{j,t}^{(\Im\{\mathbf{z}\})}$ parts of the noisy wavelet coefficients according to their individual magnitudes; this is essentially [1] applied to both real and imaginary parts. The second approach, called here *analytic thresholding* [17], involves creating synthetic analytic signals $\mathbf{a} = \Re\{\mathbf{z}\} + i\mathcal{H}\Re\{\mathbf{z}\}$ and $\mathbf{b} = \Im\{\mathbf{z}\} + i\mathcal{H}\Im\{\mathbf{z}\}$ and separately thresholding the real $W_{j,t}^{(\Re\{\mathbf{z}\})}$ and imaginary $W_{j,t}^{(\Im\{\mathbf{z}\})}$ parts of the noisy wavelet coefficients according to the magnitudes of $W_{j,t}^{(\mathbf{a})}$ and $W_{j,t}^{(\mathbf{b})}$, respectively. This approach preserves phase relationships between the real-valued components. In the third alternative, *Sardy's thresholding* [14], we threshold the complex-valued noisy wavelet coefficients $W_{j,t}^{(\mathbf{z})}$ depending on their magnitudes.

B. Synthetic Noisy Signals

We use throughout the "least asymmetric" Daubechies filter of width $L = 8$. Results are for series lengths $N = 512$ and 1024. The stationary wavelet transform is carried out to level $J_0 = 6$ so that, as is common practice, low frequencies are not subjected to thresholding. We took a signal-variance-to-noise-variance ratio, i.e., signal-to-noise variance ratio, of 50 (almost identical to the standard deviation ratio of 7 used

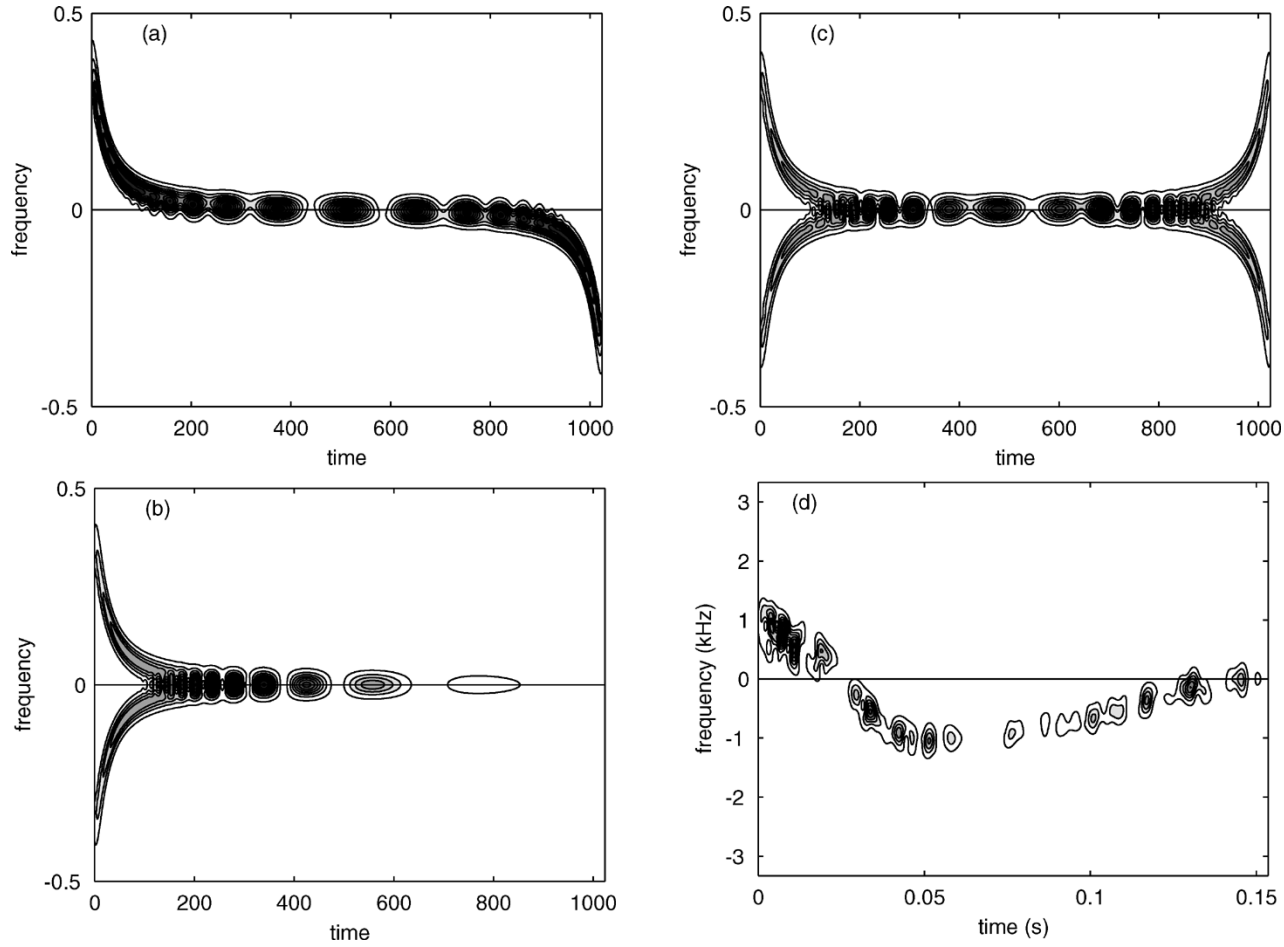

Fig. 4. (a)–(d) Hermite window spectrograms for signals 1–4.

in [1]). The first three models for $\mathbf{d}$ are based around complex-valued variations to the real Doppler signal in [1], as follows:

$$d_{1,t} = \left[1 - \left(\frac{t}{N}\right)\right] \exp\left\{\frac{-i2\pi 1.05}{\left[\left(\frac{t}{N}\right) + 0.05\right]}\right\} + \left(\frac{t}{N}\right) \exp\left\{\frac{-i2\pi 1.05}{\left[-\left(\frac{t}{N}\right) + 1.05\right]}\right\}$$

$$d_{2,t} = \frac{\left[1 - \left(\frac{t}{N}\right)\right](1+i)}{\sqrt{2}} \sin\left\{\frac{2\pi 1.05}{\left[\left(\frac{t}{N}\right) + 0.05\right]}\right\}$$

$$d_{3,t} = \left[1 - \left(\frac{t}{N}\right)\right] \cos\left\{\frac{2\pi 1.05}{\left[\left(\frac{t}{N}\right) + 0.05\right]}\right\} + i\left(\frac{t}{N}\right) \sin\left\{\frac{2\pi 1.05}{\left[-\left(\frac{t}{N}\right) + 0.05\right]}\right\}.$$

The fourth signal is a Wang–Fish simulation [18] of a quadrature Doppler ultrasound recording of blood flow in the femoral artery.

One hundred independent simulations of each noisy signal were made, and for each case, denoising was carried out using standard, analytic, Sardy's, and local directional thresholding. Table I shows the average and standard error over the 100 trials of the mean-square error between signal and estimator, given as a proportion of σ_ϵ^2. A robust estimate of σ_ϵ was used (see, e.g., [6, p. 429]).

The Hermite spectrograms of all four noise-free signals are shown in Fig. 4. Signals 1 and 4 both exhibit strong local directionality determined by the phase relationships between their real and imaginary parts. The combination of the local directionality and the beneficial energy unbalancing action of the MODWT [e.g., Fig. 3(a)–(d)] results in local directional thresholding outperforming analytic and Sardy's thresholding, with standard thresholding further behind.

TABLE I
AVERAGE (STANDARD ERROR) OF [MEAN-SQUARE ERROR/σ_ϵ^2] FOR SIGNALS 1–4 AND THE FOUR THRESHOLDING METHODS. TOP BLOCK FOR $N = 512$, AND BOTTOM BLOCK FOR $N = 1024$

	Standard	*Sardy*	*LocalDir.*	*Analytic*
1	0.35 (0.03)	0.29 (0.02)	0.27 (0.02)	0.28 (0.02)
2	0.21 (0.02)	0.17 (0.02)	0.18 (0.02)	0.18 (0.02)
3	0.21 (0.02)	0.27 (0.02)	0.29 (0.02)	0.18 (0.02)
4	0.98 (0.08)	0.80 (0.08)	0.41 (0.03)	0.81 (0.08)
1	0.23 (0.02)	0.18 (0.01)	0.12 (0.01)	0.18 (0.01)
2	0.13 (0.01)	0.10 (0.01)	0.11 (0.01)	0.11 (0.01)
3	0.13 (0.01)	0.18 (0.01)	0.19 (0.01)	0.11 (0.01)
4	0.69 (0.04)	0.55 (0.03)	0.32 (0.02)	0.56 (0.04)

Signal 2 has identical real and imaginary parts at any time. The magnitude of the complex signal is thus large whenever the individual real and imaginary parts are large. However, at any time, the signal has both positive and negative frequency contributions, so no advantage accrues to local directional thresholding. Sardy's thresholding slightly outperforms both the analytic and local directional thresholding, again with standard thresholding in fourth place. With equal real and imaginary parts, the analytic thresholding does the same threshold tests for both components: Sardy's thresholding benefits from the fact that only N thresholding tests are carried out compared with $2N$ with the alternative methods.

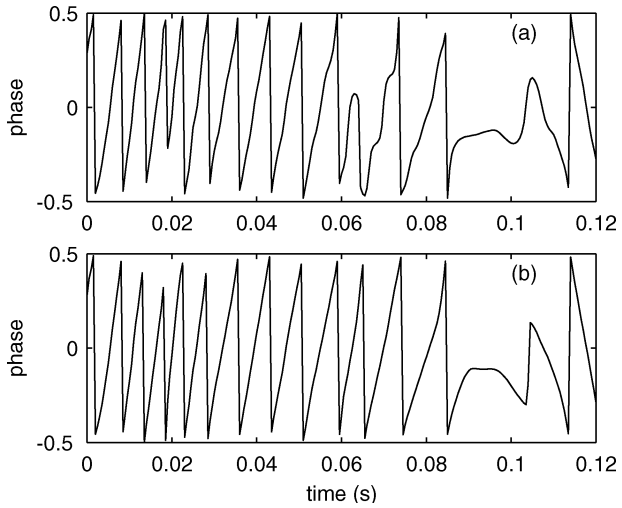

Fig. 5. Phase constructed from thresholded Hepatic vein data using (a) Sardy's and (b) local directional thresholding.

Signal 3 has real and imaginary parts related in a way that does not define a useful complex amplitude and phase for $\mathbf{d}_3$ and at any time has both positive and negative frequency contributions. We would thus expect thresholding methods that treat the real-valued components separately to perform best, and this is seen to be true. Both the analytic and standard methods significantly outperform the intrinsically complex approaches of Sardy or local directional thresholding.

C. Actual Noisy Signal

Finally, we return to the hepatic vein data of Fig. 3. This already-noisy complex-valued series, of length 776, was processed exactly as for the synthetic examples. We can reparameterize the thresholded values $\hat{z}_t$ in terms of amplitude and phase as $\hat{z}_t = a_t \exp(i2\pi\varphi_t)$, where of course $a_t = \sqrt{[(\Re\{\hat{z}_t\})^2 + (\Im\{\hat{z}_t\})^2]}$, and $\varphi_t = (1/[2\pi]) \tan^{-1}(\Im\{\hat{z}_t\}/\Re\{\hat{z}_t\})$, enabling us to assess these aspects of the relationships between the real and imaginary parts. Fig. 2 suggests a change from positive to negative frequencies (positive to reverse directionality) around 0.1 s. Fig. 5 compares the (wrapped) phase resulting from Sardy's thresholding and local directional thresholding for times leading up to and slightly beyond this directional change-point. (Standard and analytic thresholding gives a very similar result to Sardy's thresholding.) We see that local directional thresholding produces a better defined and more predictable phase behavior; in fact, it also produces the smoothest amplitude behavior.

VI. Conclusion

Denoising of complex-valued signals via wavelet thresholding is a nontrivial extension to denoising of real-valued signals. Some signals have physically well-defined real/imaginary relationships; e.g., quadrature Doppler ultrasound is bidirectional overall but unidirectional at any one time. For these locally directional signals, we introduced the idea of local directional thresholding and illustrated its efficacy on synthetic and real data. We note that Doppler ultrasound signals and other familiar directional complex-valued signals, such as in seismology, are inhomogeneous but smooth.

The spectrogram can be used to test for local directionality. If the signal at some time is present at negative or positive frequencies and crosses the axis $f = 0$, it is locally directional; our approach is tuned for this case. If not, other methods will be competitive/better as seen in the simulations.

Acknowledgment

The authors would like to thank J. Jensen for permission to use the hepatic vein data, and the Associate Editor and referees for constructive comments leading to an improved exposition.

References

[1] D. L. Donoho and I. M. Johnstone, "Ideal spatial adaption by wavelet shrinkage," *Biometrika*, vol. 81, pp. 425–55, 1994.

[2] ——, "Adapting to unknown smoothness via wavelet shrinkage," *J. Amer. Stat. Assoc.*, vol. 90, pp. 1200–24, 1995.

[3] R. R. Coifman and D. L. Donoho, "Translation-invariant denoising," in *Wavelets and Statistics*, A. Antoniadis and G. Oppenheim, Eds. New York: Springer-Verlag, 1995, vol. 103, Lecture Notes in Statistics, pp. 125–50.

[4] G. P. Nason and B. W. Silverman, "The stationary wavelet transform and some statistical applications," in *Wavelets and Statistics*, A. Antoniadis and G. Oppenheim, Eds. New York: Springer-Verlag, 1995, vol. 103, Lecture Notes in Statistics, pp. 281–99.

[5] M. Lang, H. Guo, J. E. Odegard, C. S. Burrus, and R. O. Wells, "Noise reduction using an undecimated discrete wavelet transform," *IEEE Signal Process. Lett.*, vol. 3, no. 1, pp. 10–2, Jan. 1996.

[6] D. B. Percival and A. T. Walden, *Wavelet Methods for Time Series Analysis*. Cambridge, U.K.: Cambridge Univ. Press, 2000.

[7] S. C. Olhede and A. T. Walden, "Polarization phase relationships via multiple Morse wavelets. II. Data analysis," in *Proc. R. Soc. Lond. A, Math. Phys. Sci.*, vol. 459, 2003, pp. 641–57.

[8] D. H. Evans, W. N. McDicken, R. Skidmore, and J. P. Woodcock, *Doppler Ultrasound: Physics, Instrumentation and Clinical Applications*. Chichester, U.K.: Wiley, 1989.

[9] M. A. Poletti, "The homomorphic analytic signal," *IEEE Trans. Signal Process.*, vol. 45, no. 8, pp. 1943–1953, Aug. 1997.

[10] M. Bayram and R. Baraniuk, "Multiple window time-varying spectrum estimation," in *Nonlinear and Nonstationary Signal Processing*, W. J. Fitzgerald, R. L. Smith, A. T. Walden, and P. C. Young, Eds. Cambridge, U.K.: Cambridge Univ. Press, 2000, pp. 292–316.

[11] M. S. Sabri and W. Steenaart, "Discrete Hilbert transform filtering," *IEEE Trans. Acoust., Speech, Signal Process.*, vol. 25, no. 5, pp. 452–4, Oct. 1977.

[12] S. L. Marple Jr., "Computing the discrete-time 'analytic' signal via FFT," *IEEE Trans. Signal Process.*, vol. 47, no. 9, pp. 2600–3, Sep. 1999.

[13] F. Abramovich, Y. Benjamini, D. Donoho, and I. Johnstone, "Adapting to unknown sparsity by controlling the false discovery rate," Dept. of Statistics, Stanford Univ., , Tech. Rep. 2000-19, 2000.

[14] S. Sardy, "Minimax threshold for denoising complex signals with waveshrink," *IEEE Trans. Signal Process.*, vol. 48, no. 4, pp. 1023–8, Apr. 2000.

[15] T. R. Downie and B. W. Silverman, "The discrete multiple wavelet transform and thresholding methods," *IEEE Trans. Signal Process.*, vol. 46, no. 9, pp. 2558–61, Sep. 1998.

[16] S. Barber and G. P. Nason, "Real nonparametric regression using complex wavelets," *J. R. Statist. Soc. B.*, vol. 66, pp. 927–39, 2004.

[17] S. C. Olhede and A. T. Walden, "'Analytic' wavelet thresholding," *Biometrika*, vol. 91, pp. 955–73, 2004.

[18] ——, "Noise reduction in directional signals using multiple Morse wavelets illustrated on quadrature Doppler ultrasound," *IEEE Trans. Biomed. Eng.*, vol. 50, no. 1, pp. 51–57, Jan. 2003.